Photochemistry and Photobiology, 2012, 88: 38–45

Slow Solvent Relaxation Dynamics of Nanometer Sized Reverse Micellar Systems Through Tryptophan Metabolite, Kynurenine

Surajit Rakshit, Nirmal Goswami and Samir Kumar Pal*

Unit for Nano Science & Technology, Department of Chemical, Biological & Macromolecular Sciences, S. N. Bose National Centre for Basic Sciences, Block JD, Sector III, Salt Lake, Kolkata 700098, India

Received 1 July 2011, accepted 23 September 2011, DOI: 10.1111/j.1751-1097.2011.01007.x

ABSTRACT

Exploration of environmental dynamics using intrinsic biological probe tryptophan is very important; however, it suffers from various difficulties. An alternative probe, kynurenine (KN), has been found to be an efficient probe for the ultrafast dynamics in the biological environment (Goswami *et al.*, [2010] *J. Phys. Chem. B.*, 114, 15236–15243). In the present study, we have investigated the efficacy of KN for the exploration of relatively slower dynamics of biologically relevant environments. A detailed investigation involving UV–Vis, steady-state/time-resolved fluorescence spectroscopy and Förster resonance energy transfer (FRET) studies on KN compared to a well-known solvation probe, H33258, a DNA-minor groove binder in a model nonionic reverse micelle reveals that ultrafast internal conversion associated with the hydrogen-bonding dynamics masks KN to become a dynamical reporter of the immediate environments of the probe.

INTRODUCTION

Tryptophan (Trp) is the most important fluorophore among all the amino acids, which has been extensively used for decades to study protein dynamics by measuring the quantum yield, fluorescence lifetime and time-resolved anisotropy and widely utilized in electron transfer or resonance energy transfer studies in proteins (1–3). However, despite the large number of studies, critical wavelength of excitation (295–300 nm), ultrafast internal conversion (IC), low quantum yield make Trp as probe to be a bit difficult (2). Kynurenine (KN) is one of the Trp metabolites and omnipresent in the lens of human eyes in order to protect the retina from possible UV (300–400 nm) radiation damage (4) and can be used as an alternative of Trp (1). A systematic study on the spectroscopy and dynamics of KN in different solvents has been presented by Sherin *et al.* (5). It has been demonstrated that KN exhibits very fast decay in polar solvents where IC has been shown to be the main deactivation channel (5,6). In this regard, it would be interesting to investigate the ability of the probe KN for the exploration of relatively slower dynamics, which may prevail in the cavity/cleft of various proteins. However, any study focusing on the exploration of relatively slower solvent dynamics using KN as a potential probe in the biologically relevant restricted media is sparse in the present literature. Nanometer-sized water pools of reverse micellar (RM) systems are found to be an excellent mimic of such biomolecular cavity/cleft (7). Therefore, a complete study on the interaction of this fluorophore (KN) with biomimicking systems (RMs) is strongly demanding and is the goal of the present work. The entrapped water inside the RM core has properties interestingly different from those in the bulk and provides a potential platform to understand the dynamic property of water in real biological systems.

In the present study, we report a detailed photophysical characterization of KN with model nonionic tetraethylene glycol monododecyl ether (Brij-30) RM. We have employed a dynamic light scattering (DLS) study for the structural characterization of the RM. Steady state, picosecond-resolved optical spectroscopy including polarization-gated fluorescence anisotropy studies reveal the dynamics of the probe and solvent relaxation in the nanopool of water in the RM. In order to investigate the intermediate photoinduced species of the probe KN we have used picosecond-resolved area normalized emission spectroscopy (TRANES). Förster resonance energy transfer (FRET) studies of the probe to another surface bound acceptors, crystal violet (CV) and coumarin 500 (C500) confirm interfacial binding of the probe KN in the RM. In order to compare the dynamical information of the RM environments as revealed by the probe KN, we have also used another well-known solvation probe H33258 (a DNA minor groove binder [8–10]) for the exploration of solvent relaxation in the restricted environments. Our detailed spectroscopic studies on the very important probe KN in the biologically relevant organized assemblies may find relevance in the use of the probe for the investigation of slower photoinduced dynamical events in biologically important restricted environments.

MATERIALS AND METHODS

D, L-KN, Isooctane (i-Oc), Hoechst 33258 (H33258) and CV were purchased from Sigma/Aldrich and used as received. Brij 30 and C500 were from Fluka and Exciton, respectively. Double-distilled water was used for preparation of RM of different w_0 values. To prepare the RM of w_0 = 0, Brij 30 was dissolved in i-Oc to make the final concentration 200 mM and calculated amount of water (5.94 μL for w_0 = 1.1 and 10.8 μL for w_0 = 2) were added to prepare the RM of higher w_0 values. It has to be mentioned that although we have not added any amount of water in the RM of w_0 = 0, the presence of some residual water cannot be excluded (11). For the energy-transfer experiments, the donor (KN) concentration was 10 μM, whereas the concentration of CV and C500 were 300 μM and 600 μM, respectively. It has to be noted that the micellar concentration (*ca* mM) is higher than that of the acceptor molecules.

*Corresponding Author email: skpal@bose.res.in (Samir Kumar Pal)

Steady-state absorption and emission were measured with a Shimadzu UV-2450 spectrophotometer and Jobin Yvon Fluoromax-3 fluorimeter, respectively. DLS measurements were carried out with Nano-S Malvern instrument employing a 4 mW, He–Ne laser (λ = 632.8 nm) equipped with a thermostated sample chamber. Hydrodynamic diameter (d_H) of the RM is estimated from the intensity autocorrelation function of the time-dependent fluctuation in intensity. d_H is defined as,

$$d_H = \frac{k_b T}{3\pi\eta D}, \tag{1}$$

where k_b is the Boltzmann constant, η is the viscosity and D is the translational diffusion coefficient.

Fluorescence decay transients were measured and fitted by using a commercially available spectrophotometer (LifeSpec-ps) from Edinburgh Instruments (UK) (excitation wavelengths of 375 nm and 409 nm with 60 ps instrument response function [IRF]). The observed fluorescence transients were fitted by using a nonlinear least squares fitting procedure to a function ($X(t) = \int_0^t E(t')R(t-t')\mathrm{d}t'$) comprising convolution of the IRF ($E(t)$) with a sum of exponentials ($R(t) = A + \Sigma_{i=1}^{N} B_i e^{-t/\tau_i}$) with pre-exponential factors (B_i), characteristic lifetimes (τ_i; the lifetime τ is the time needed for the concentration of molecular entities to decrease to $1/e$ of its original value as per the equation $I = I_0 \exp(t/\tau)$) and a background (A). Relative concentration in a multiexponential decay was finally expressed as $a_n = B_n/\Sigma_{i=1}^{N} B_i$. The quality of the curve fitting was evaluated by reduced chi-square (χ^2) and residual data.

To construct time-resolved emission spectra (TRES) we followed the technique described in Refs. 12 and 13. As described above the emission intensity decays are analyzed in terms of the multiexponential model,

$$I(\lambda, t) = \sum_{i=1}^{N} \alpha_i(\lambda) \exp[-t/\tau_i(\lambda)], \tag{2}$$

where $\alpha_i(\lambda)$ are the pre-exponential factors, with $\sum \alpha_i(\lambda) = 1.0$. In this analysis, we computed a new set of intensity decays, which were normalized so that the time-integrated intensity at each wavelength is equal to the steady-state intensity at that wavelength. Considering $F(\lambda)$ to be the steady-state emission spectrum, we calculated a set of $H(\lambda)$ values using,

$$H(\lambda) = \frac{F(\lambda)}{\int_0^\infty I(\lambda, t)\mathrm{d}t} \tag{3}$$

which for multiexponential analysis becomes,

$$H(\lambda) = \frac{F(\lambda)}{\sum_i \alpha_i(\lambda)\tau_i(\lambda)} \tag{4}$$

Then, the appropriately normalized intensity decay functions were given by,

$$I'(\lambda, t) = H(\lambda)I(\lambda, t) = \sum_{i=1}^{N} \alpha'(\lambda) \exp\left(\frac{-t}{\tau_i(\lambda)}\right) \tag{5}$$

where $\alpha'_i(\lambda) = H(\lambda)\alpha_i(\lambda)$. The values of $I'(\lambda,t)$ were used to calculate the intensity at any wavelength and time, and thus the TRES. The values of the emission maxima and spectral width were determined by nonlinear least-squares fitting of the spectral shape of the TRES. The spectral shape is assumed to follow a lognormal line shape,

$$I(\bar{\nu}) = I_0 \exp\left\{-\left[\ln 2\left(\frac{\ln(\alpha+1)}{b}\right)^2\right]\right\} \tag{6}$$

with $\alpha = \frac{2b(\bar{\nu}-\bar{\nu}_{max})}{b} > -1$, where I_0 is amplitude, $\bar{\nu}$ is the wavenumber of the emission maximum and spectral width is given by $\Gamma = \Delta[\sinh(b)/b]$. The terms b and Δ are asymmetry and width parameters and the Eq. (6) reduces to a Gaussian function for $b = 0$.

The time dependent fluorescence Stokes shifts, as estimated from TRES (12,13), were used to construct the normalized spectral shift correlation function or the solvent correlation function $C(t)$ defined as

$$C(t) = \frac{\nu(t) - \nu(\infty)}{\nu(0) - \nu(\infty)}, \tag{7}$$

where $\nu(0)$, $\nu(t)$ and $\nu(\infty)$ are the emission maximum (in cm^{-1}) at time zero, t and infinity respectively. The $\nu(\infty)$ values had been taken to be the emission frequency beyond which an insignificant or no spectral shift was observed. The $C(t)$ function represents the temporal response of the solvent relaxation process, as occurs around the probe following its photoexcitation and the associated change in the dipole moment. To ascertain the heterogeneity in the location of KN in the RM, we further followed the time-resolved area normalized emission spectral (TRANES) technique (14,15). TRANES is a model-free modified version of TRES mentioned earlier. A useful feature of the method is that an isoemissive point in the spectra involves two emitting species (could be same molecule in different environments), which are kinetically coupled either irreversibly or reversibly or not coupled at all. For fluorescence anisotropy ($r(t)$) measurements, emission polarization was adjusted to be parallel or perpendicular to that of the excitation and the anisotropy is defined as,

$$r(t) = \frac{[I_{Para}(t) - G \times I_{Perp}(t)]}{[I_{Para}(t) + 2 \times G \times I_{Perp}(t)]} \tag{8}$$

G is the grating factor, was determined following longtime tail matching technique (16). All the fluorescence anisotropies were measured at the emission maxima.

To estimate the FRET efficiency of the donor and hence to determine the distance of the donor–acceptor (DA) pair, we followed the methodology described in chapter 13 of Ref 13. The Förster distance (R_0) is given by

$$R_0 = 0.211[\kappa^2 n^{-4} Q_D J(\lambda)]^{1/6} \quad (\text{in } \mathring{A}), \tag{9}$$

where κ^2 is a factor describing the relative orientation in space of the transition dipoles of the donor and acceptor. In the present study, the acceptor CV can bind at the surface of the RM at any orientation with respect to the donor KN. Thus, for an ensemble of D–A pairs the relative orientation of the D–A is not supposed to be constant. We assumed that the orientation factor κ^2 is equal to the dynamic average of 2/3, which is not a major deviation from real fact of randomized donor and acceptor orientations in an ensemble. Moreover, variation of κ^2 does not seem to have resulted in major errors in the calculated distances (17). The refractive index (n) of the medium is measured to be 1.39. $J(\lambda)$, the overlap integral, which expresses the degree of spectral overlap between the donor emission and the acceptor absorption is given by

$$J(\lambda) = \frac{\int_0^\infty F_D(\lambda)\varepsilon(\lambda)\lambda^4\mathrm{d}\lambda}{\int_0^\infty F_D(\lambda)\mathrm{d}\lambda}, \tag{10}$$

where $F_D(\lambda)$ is the fluorescence intensity of the donor in the wavelength range of λ to $\lambda + \mathrm{d}\lambda$ and is dimensionless. $\varepsilon(\lambda)$ is the extinction coefficient (in $M^{-1}\ cm^{-1}$) of the acceptor at λ. If λ is in nanometers, then $J(\lambda)$ is in units of $M^{-1}\ cm^{-1}\ nm^4$.

Q_D, the quantum yield of the donor in the absence of acceptor, was calculated according to the following equation:

$$Q = Q_R\left(\frac{I}{I_R}\right)\left(\frac{OD_R}{OD}\right)\left(\frac{n^2}{n_R^2}\right), \tag{11}$$

where Q and Q_R are the quantum yield of KN in the RM of different w_0 values and reference (protein-bound KN). I and I_R are the integrated fluorescence intensities of KN in the RM of different w_0 values and reference respectively. OD and OD_R are the optical densities of KN in the RM of different w_0 values and reference at the excitation wavelength 375 nm and n and n_R are the refractive indices of KN in the RM of different w_0 values and reference solutions respectively. The

absolute quantum yield of protein bound KN (1) was taken to be 4.8×10^{-3}. Refractive indices of the solutions were measured by using Rudolph J357 automatic refractometer.

Once the value of R_0 is known, the D–A distance (R) can easily be calculated using the formula,

$$R^6 = [R_0^6(1 - E)/E] \quad (12)$$

Here, E is FRET efficiency, measured by using the lifetimes of the donor in the absence τ_D and presence τ_{DA} of acceptor which is defined as

$$E = 1 - \tau_{DA}/\tau_D \quad (13)$$

It has to be noted that Eq. 13 holds rigorously only for a homogeneous system (*i.e.* identical D–A complexes) in which the donor and the D–A complex have single-exponential decays. However, for D–A systems decaying with multiexponential lifetimes, FRET efficiency (E) is calculated from the amplitude-weighted lifetimes $\langle\tau\rangle = \sum \alpha_i \tau_i$ where α_i is the relative amplitude contribution to the lifetime τ_i values (13). We have used the amplitude-weighted time constants for τ_D and τ_{DA} to evaluate E using Eq. 13.

RESULTS AND DISCUSSION

Figure 1a depicts the results obtained from DLS measurement of Brij 30 RM in i-Oc at different w_0 values. It can be observed that Brij 30 RM produces spherical and monodispersed droplets with a hydrodynamic diameter of 7.8 nm for $w_0 = 0$. As w_0 increases, the hydrodynamic diameter of the RM increases due to the increase of water pool size. Inset of Fig. 1b shows the absorbance of KN in the RM at $w_0 = 0$ (dash line) and the empty RM (gray line). The broadening of the absorption spectrum of KN could be due to the existence of KN at different locations, as empty RM are not supposed to absorb at this wavelength region. Emission spectra of KN in the RM with different w_0 values are shown in Fig. 1b. A small redshift in the absorption spectrum and a significant blueshift in the emission spectrum compared to KN in water (5) due to the stabilization of excited state energy on varying the nature of the solvent, reveal the binding of KN with the RM. KN exhibits the emission spectrum with three shoulders at around 410, 435 and 460 nm respectively, which may be due to different locations of the probe in the RM system (5). The emission peak at 460 nm corresponds to KN in the polar region of associated water molecules (pool) in the RM (18); 435 nm stands for the probe near the polar head groups of Brij 30 and the small water pool which is similar to protein bound KN (19), whereas 410 nm corresponds to KN in the interface between Brij 30 and i-Oc due to maximum destabilization of S_1 state (5). We have also checked that the empty RM has no emission at this wavelength region which excludes the possibility of any contribution from empty RM (Figure S1). We have also recorded excitation spectra (inset of Fig. 1b) at different selected wavelengths over the whole emission spectrum of KN in the RM (Figure S2). The overall similarity of the excitation spectra except for the shift of maxima (*ca* 3 nm) due to the heterogeneity in the location of KN and their consistency with the corresponding absorption spectra (inset of Fig. 1b) clearly rule out the possibility of fluorescence signal from impurities in the sample.

The decay transients of KN bound to the RM have been studied at 14 different wavelengths, starting from 400 to 530 nm throughout the emission spectra for different w_0

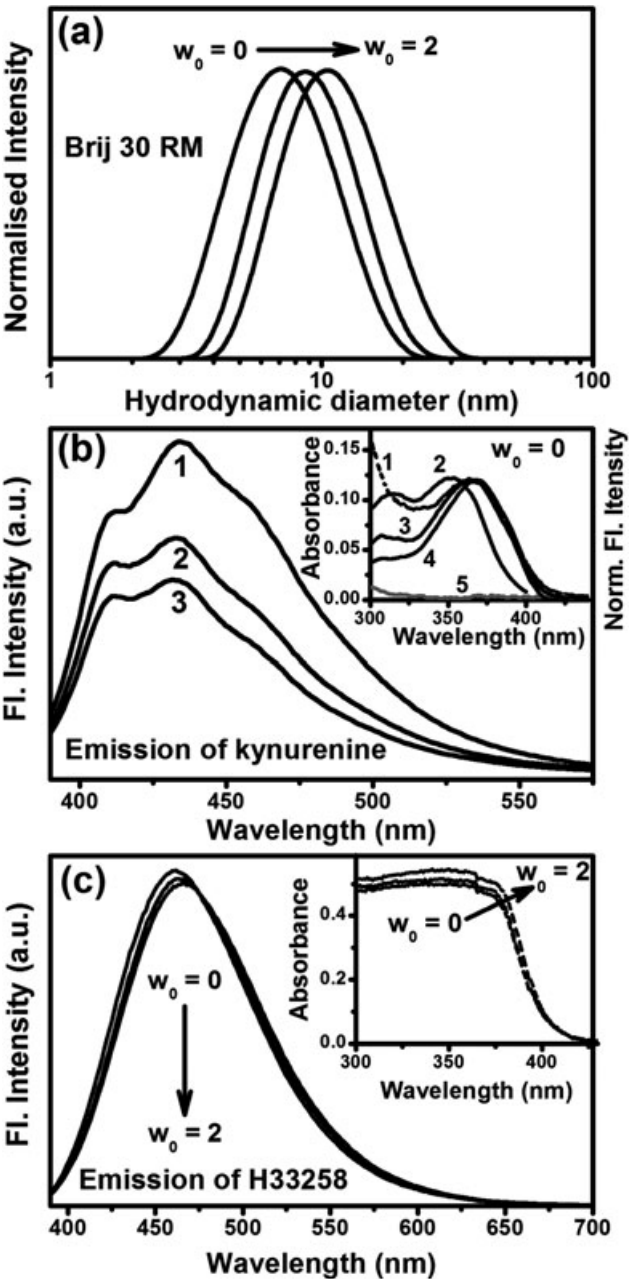

Figure 1. (a) Hydrodynamic diameter of Brij-30/isooctane/water reverse micellar systems with $w_0 = 0.0$, 1.1 and 2.0. (b) Emission spectra ($\lambda_{ex} = 375$ nm) of KN in reverse micelles at $w_0 = 0$ (1), $w_0 = 1.1$ (2) and $w_0 = 2$ (3), respectively. Inset. Isooctane subtracted absorption spectra of the empty RM (solid gray line, 5) and KN at $w_0 = 0$ (dash line, 1). Normalized excitation spectra of KN (solid line) with $w_0 = 0$ monitored at 410 nm (2), 430 nm (3) and 460 nm (4) are also presented in the inset. (c) Emission ($\lambda_{ex} = 375$ nm) and absorption (inset) spectra of H33258 in the nano-cavity of reverse micelle at different w_0 values. KN = kynurenine.

values. Figure 2a represents the fluorescence decay transients of KN in Brij 30 RM of $w_0 = 0$ at two different wavelengths 400 and 530 nm. On the blue edge of the spectrum (400 nm) the signal is seen to decay, whereas on the red edge (530 nm) it rises, which is the clear indication of the excited state relaxation dynamics of KN. Similar results are found for the other w_0 values (data not shown). From this family of

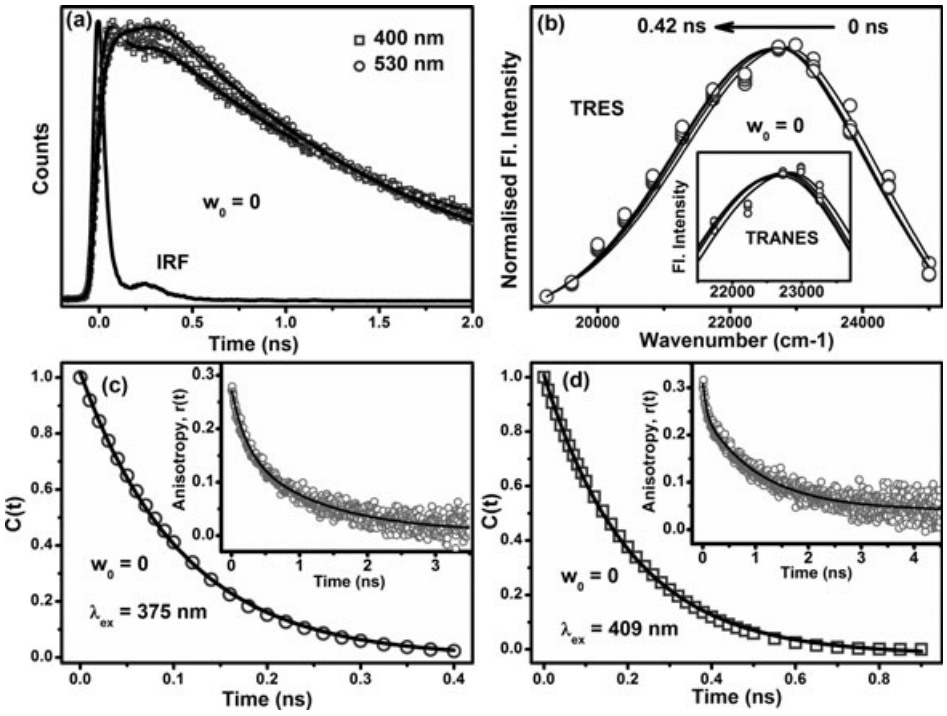

Figure 2. (a) Fluorescence transients, (b) TRES and TRANES (inset) of KN in Brij 30 RM at $w_0 = 0$. (c) and (d) Solvent relaxation dynamics and fluorescence anisotropy decay (inset) of KN in Brij 30 RM at $w_0 = 0$ at 375 and 409 nm excitation, respectively. TRES = time-resolved emission spectra; TRANES = time-resolved area normalized emission spectra; KN = kynurenine; RM = reverse micelles.

transients, we have constructed the TRES at different w_0 values. The observed dynamical Stokes shift is relatively small (160 cm^{-1}) for $w_0 = 0$ and eventually completed within 420 ps (shown in Fig. 2b). To explore the environmental dynamics of KN at different w_0 values, the temporal decay of solvent correlation function, $C(t)$ has been constructed. Figure 2c reveals the $C(t)$ decay of KN at $w_0 = 0$, which shows an apparent mono-exponential decay with time constant of 105 ps. With an increase of w_0 values, $C(t)$ becomes faster (see Table 1 and Figure S3). It could also be noted that an ultrafast component of the solvent response, which is due to the relaxation of bulk-like water (of the order of a few picoseconds) is not resolvable in our experimental setup. In order to calculate the missing spectral shift in the solvent relaxation process, we have applied the method suggested by Fee *et al.* (20). The real time-zero in the emission maximum ($\nu(t = 0)$) can be estimated from the steady-state absorption and fluorescence maxima by the following equation:

Table 1. Solvent relaxation time constants and rotational time constants of kynurenine (KN) in the reverse micellar system at various w_0 values with a standard error of *ca* 10%.

w_0	Solvation time constants τ (ps)	$\Delta\upsilon$ (cm^{-1})	Missing spectral shift	Rotational time constants τ_1 (ps)	τ_2 (ns)	τ_3 (ns)
0.0	105	160	57%	210 (39%)	1.2 (57%)	30 (4%)
1.1	54	70	63%	100 (36%)	1.0 (58%)	55 (6%)
2.0	49	66	71%	160 (36%)	1.2 (61%)	100 (4%)

$$\nu(t = 0) = \nu_p(\text{abs}) - \lfloor \nu_{np}(\text{abs}) - \nu_{np}(\text{fl}) \rfloor, \qquad (14)$$

where the subscripts "p" and "np" refer to the spectra in polar and nonpolar environments respectively. In the present study, we have used protein bound KN spectra as a nonpolar environment with absorption and emission maxima at 360 and 435 nm respectively and water is used as the polar solvent where KN shows an absorption peak at 360 nm. The percentage of missing spectral shift is $((\nu_{cal}(0) - \nu(0))/(\nu_{cal}(0) - \nu(\infty))) \times 100$. The observed time zero frequency and the time infinity frequency for KN in RM of $w_0 = 0$ are 22 778 cm^{-1} and 22 618 cm^{-1} respectively. The missing spectral shift corresponding to the unobservable solvent relaxation component for the present time resolution and the percentage of missing spectral shift are also listed in Table 1. On addition of water to the RM the missing spectral shift gradually increases. This result seems to be logical because the formation of bulk type water molecules in the pool increases upon addition of water above $w_0 = 0$, leading to faster environmental dynamics beyond the resolution of our experimental setup.

In order to investigate the existence of multiple emitting species in various environments with different excited state lifetime values leading to time-dependent spectral shift, we have employed the TRANES technique. For $w_0 = 0$ the TRANES are shown in the inset of Fig. 2b. An isoemissive point at 22 730 cm^{-1} for $w_0 = 0$ is clearly evident, revealing the possible coexistence of at least two species in the microenvironments of the RM. The observation is consistent with the fact that the probe KN may interact with water molecules in the excited state (5) by different strength revealing

distinct spectroscopic signature of emission maximum. In other words KN at the micellar interface is less likely to form hydrogen bond with water molecules (19) (emission peak *ca* 23 000 cm^{-1}) compared to that in the water pool of the RM (5) (emission peak *ca* 22 000 cm^{-1}), revealing the signature of multiple species in the excited state. The temporal decay of fluorescence anisotropy ($r(t)$) of the KN–RM complex at $w_0 = 0$ is shown in the inset of Fig. 2c. It has to be noted that the time constants associated with the decay of $r(t)$ are consistent with the geometric restriction of the probe in the restricted environments. The decay transients have been fitted triexponentially, and the results are shown in Table 1. It can be observed that the time constants are of the order of hundreds of picoseconds and a few nanoseconds, which are in the same order of magnitudes for wobbling motion and lateral diffusion respectively, similar to previous result for a coumarin dye in the Brij 30 RM systems (18). In the present analysis we have fixed the longer time constant indicative of the overall rotation of the RM and estimated from the following well-known Debye–Stokes–Einstein equation:

$$\tau = \frac{\eta V}{k_b T}, \tag{15}$$

where η is the microviscosity experienced by the probe and V is molecular volume of the RM. A minor change in the locations of the probe in the RM with various hydrations (w_0) is clearly evident from the anisotropy data (Table 1). It has to be noted that in the case of the broadening of KN absorption band, the fluorescence lifetime of KN may depend on the excitation wavelength, due to relative contributions from KN at different locations in the RM. The decay time constant of the solvent correlation function ($C(t)$) in Fig. 2d from a series of detected fluorescence transients (Figure S4) with excitation wavelength of 409 nm is found to be comparable with that of the 375 nm excitation (Fig. 2c). Similarly, the anisotropy decay at 409 nm excitation wavelength (inset of Fig. 2d) is also consistent with that at 375 nm excitation (inset of Fig. 2c).

In order to investigate the nature of relaxation dynamics as revealed by the probe KN; intermolecular hydrogen bonding in the excited state causes faster deactivation through IC or solvent stabilization (solvation), we have also studied the excited state dynamics of H33258, a well-known solvation probe in the similar restricted environments for comparison. H33258 is a positively charged dye at neutral pH with absorption and emission maxima at 345 and 500 nm, respectively (21), which binds to the surface of the Brij 30 RM revealing emission maximum at 460 nm in the RM of $w_0 = 0$ at room temperature (shown in Fig. 1c). It is seen from Fig. 1c that the peak corresponding to maximum emission shows a progressive redshift with increasing water pool size depicting more polar environments at higher w_0 values. The absorption spectra (inset in Fig. 1c) remain unaltered in the entire w_0 values, indicating insignificant perturbation in the ground state stabilization of the probe H32258 in the RM.

To construct TRES, the fluorescence transients are taken at 10 equidistant wavelengths from 400 to 550 nm throughout the emission band over time windows up to 20 ns for different w_0 values. The transients show fast decay in the blue end and rise in the red end indicative of solvent relaxation dynamics (2). The constructed TRES shows a spectral shift of 1800 cm^{-1}. To ascertain whether the associated spectral shift is due to the environmental relaxation or is associated with excited heterogeneity due to the presence of multiple species, TRANES are constructed in a similar manner as described above. Fig. 3d shows the constructed TRANES of RM-H33258 complex at

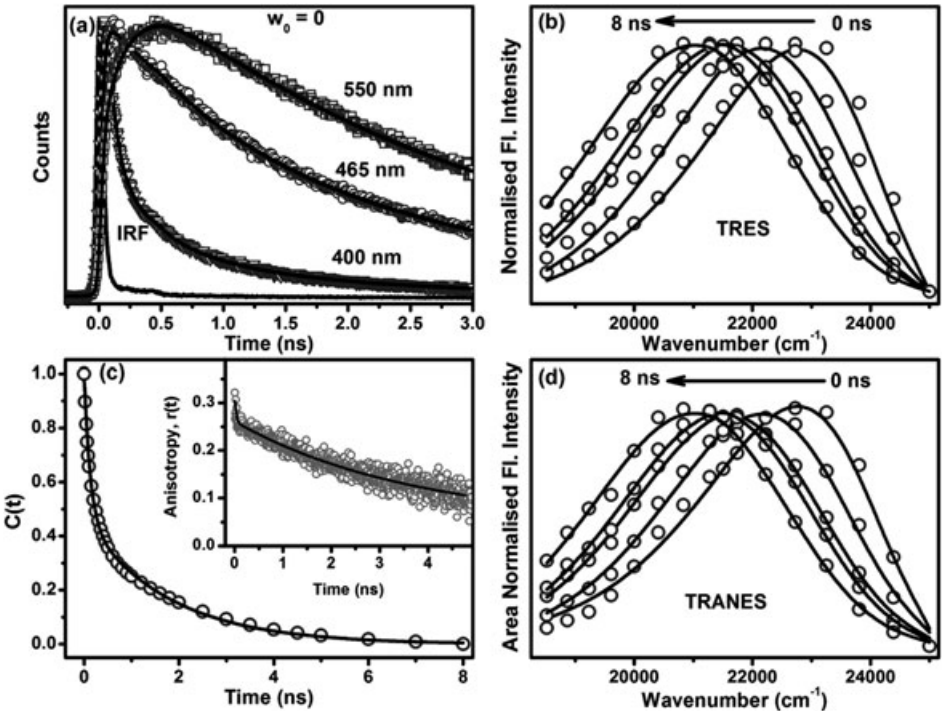

Figure 3. (a) Fluorescence transients, (b) TRES, (c) solvation correlation function and temporal decay of fluorescence (inset), (d) TRANES spectra of H33258 in Brij 30 RM at $w_0 = 0$. TRES = time-resolved emission spectra; TRANES = time-resolved area normalized emission spectra.

Table 2. Solvation correlation time constants and rotational time constants of H33258 in the reverse micellar system at various w_0 values with a standard error of *ca* 10%.

	Solvation time constants					Rotational time constants		
w_0	τ_1 (ns)	τ_2 (ns)	τ_{av} (ns)	$\Delta\upsilon$ (cm^{-1})	Missing spectral shift (%)	τ_1 (ps)	τ_2 (ns)	τ_3 (ns)
0.0	0.1 (53%)	1.8 (47%)	0.9	1800	7	200 (16%)	3.5 (65%)	30 (19%)
1.1	0.1 (56%)	1.9 (44%)	0.8	1693	11	100 (19%)	3.5 (74%)	55 (7%)
2.0	0.1 (64%)	1.4 (36%)	0.5	1627	17	90 (8%)	3.0 (88%)	100 (4%)

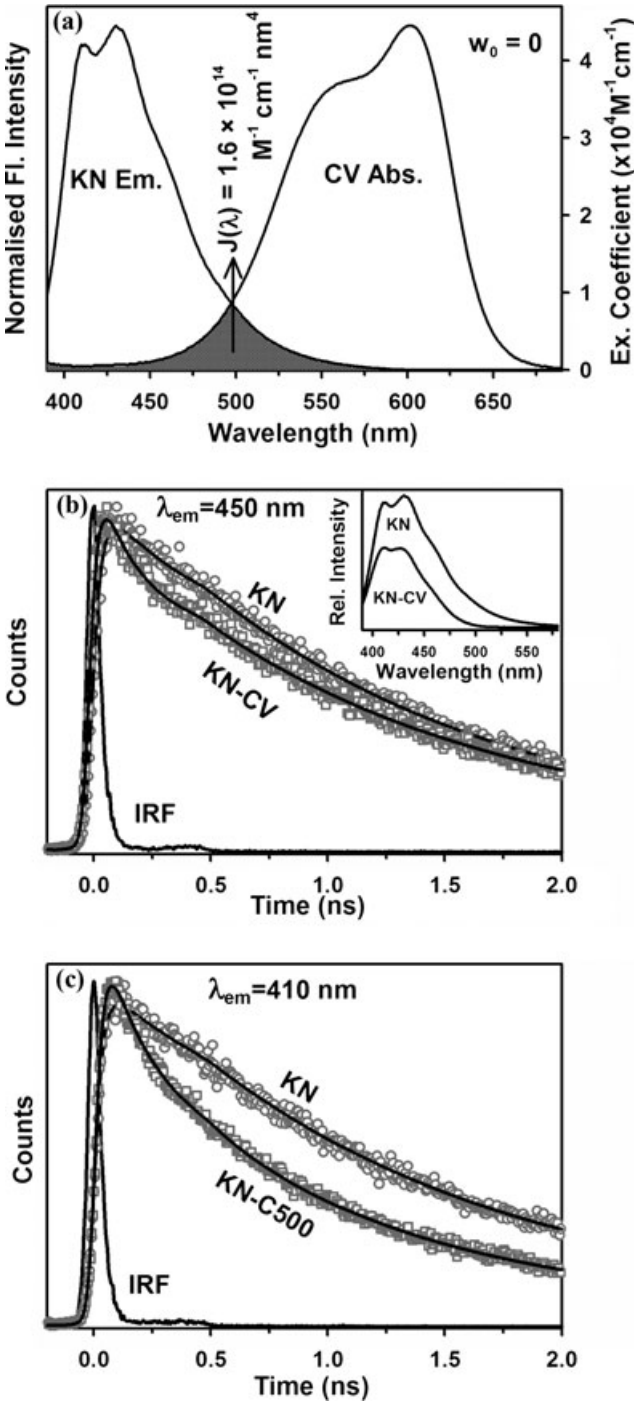

Figure 4. (a) Steady-state absorption spectrum of CV in the form of extinction coefficient and the normalized emission spectrum of KN in Brij 30 RM at $w_0 = 0$. An overlapping zone between emission of KN and absorption of acceptor CV is indicated as a gray-shaded zone. (b) Picosecond-resolved fluorescence transients of KN in the absence and in the presence of acceptor CV (excitation at 375 nm) collected at 450 nm. Inset of panel (b) shows the steady-state emission spectrum of KN in Brij 30 RM at $w_0 = 0$ in the presence and absence of CV. (c) Picosecond-resolved fluorescence transients of KN in the absence and in the presence of acceptor C500 (excitation at 375 nm) collected at 410 nm. CV = crystal violet; KN = kynurenine; RM = reverse micelles; C500 = coumarin 500.

$w_0 = 0$. The absence of isoemissive point in the TRANES is indicative of a single conformer in the relaxation process, and the measured dynamics indeed reflects environmental stabilization (solvation). The solvation correlation function (Fig. 3c) shows biexponential decay with time constants of 0.1 ns (53%) and 1.8 ns (47%), respectively, consistent with the previous studies (8). These solvent relaxation time constants are much slower than H33258 in free aqueous solution (195 fs and 1.2 ps) as reported by Pal *et al.* (10). Faster and slower components might be attributed to those water molecules near the polar head group of Brij 30 and in the central region of the water pool respectively. The temporal nature of $r(t)$s at different w_0 values (Table 2) are similar, which confirms the residence of the probe at the micellar surface. Thus, it could be concluded that the environmental dynamics as reported by H33258 are far off from that of the dynamics as probed by KN with faster IC.

In order to establish the binding position of KN into the micellar environment, we have used FRET associated with the nonradiative transfer of excited state energy from the donor fluorophore KN to the surface bound organic dyes, CV (22) and C500 (18), respectively. Figure 4a shows the considerable spectral overlap of the probe KN emission with the absorption spectrum of CV, suggesting the possibility of FRET. The significant quenching in the steady-state emission and picosecond-resolved fluorescence transient (at 450 nm) as a consequence of the D–A dipolar interaction is clearly evident from Fig. 4b. For the estimation of the FRET efficiency, we have considered the faster time constants of the D–A pair, which was absent in the donor emission in absence of the acceptor molecules. We have estimated the FRET efficiency to be 94% (for 29% donor population) and the characteristic Förster distance, R_0 of 2.4 nm. From FRET dynamics, the estimated effective distance (R) between the donor (KN) and the acceptor (CV) is found to be 1.5 nm. As evident in Table 3, the change in D–A distance with the increase of w_0 clearly indicates the redistribution of

Table 3. Time-resolved fluorescence decay (excitation at 375 nm and collected at 450 nm) and FRET data of KN in RM at different w_0 values in the absence and presence of CV. Values in parentheses represent the relative weight percentage of the time component with a standard error of *ca* 10%.

w_0	System	τ_1 (ps)	τ_2 (ps)	τ_3 (ps)	$<\tau_D>$ (ps)	Q_D	$J(\lambda)$ M^{-1} cm^{-1} nm^4	E (%)	R_0 (nm)	R (nm)
0	KN		1230 (94%)	6120 (6%)	1530	78.64×10^{-3}				
	KN-CV	90 (29%)	1220 (65%)	5900 (6%)			1.6×10^{14}	94	2.4	1.5
1.1	KN		1165 (91%)	5150 (9%)	1520	30.78×10^{-3}				
	KN-CV	715 (45%)	1130 (49%)	5460 (6%)			1.8×10^{14}	95	2.1	1.3
2	KN		1150 (91%)	4860 (9%)	1485	16.10×10^{-3}				
	KN-CV	630 (49%)	1120 (45%)	5100 (6%)			1.9×10^{14}	96	1.9	1.1

FRET = Förster resonance energy transfer; KN = kynurenine; RM = reverse micelles; CV = crystal violet.

Table 4. Time-resolved fluorescence decay (excitation at 375 nm and collected at 410 nm) and FRET data of KN in RM at different w_0 values in the absence and presence of C500. Values in parentheses represent the relative weight percentage of the time component with a standard error of *ca* 10%.

w_0	System	τ_1 (ps)	τ_2 (ps)	τ_3 (ps)	τ_4 (ps)	$<\tau_D>$ (ps)	$J(\lambda)$ M^{-1} cm^{-1} nm^4	E	R_0 (nm)	R (nm)
0	KN			1220 (88%)	5050 (12%)	1680				
	KN-C500	140 (28%)	540 (26%)	1230 (41%)	4460 (5%)		1.5×10^{14}	89%	2.4	1.6
1.1	KN			1230 (88%)	5210 (12%)	1690				
	KN-C500	110 (25%)	520 (28%)	1300 (43%)	5020 (4%)		1.6×10^{14}	90%	2.1	1.5
2	KN			1255 (88%)	5600 (12%)	1760				
	KN-C500	100 (19%)	470 (28%)	1290 (49%)	5100 (4%)		1.5×10^{14}	91%	1.8	1.2

FRET = Förster resonance energy transfer; KN = kynurenine; RM = reverse micelles; C500 = coumarin 500.

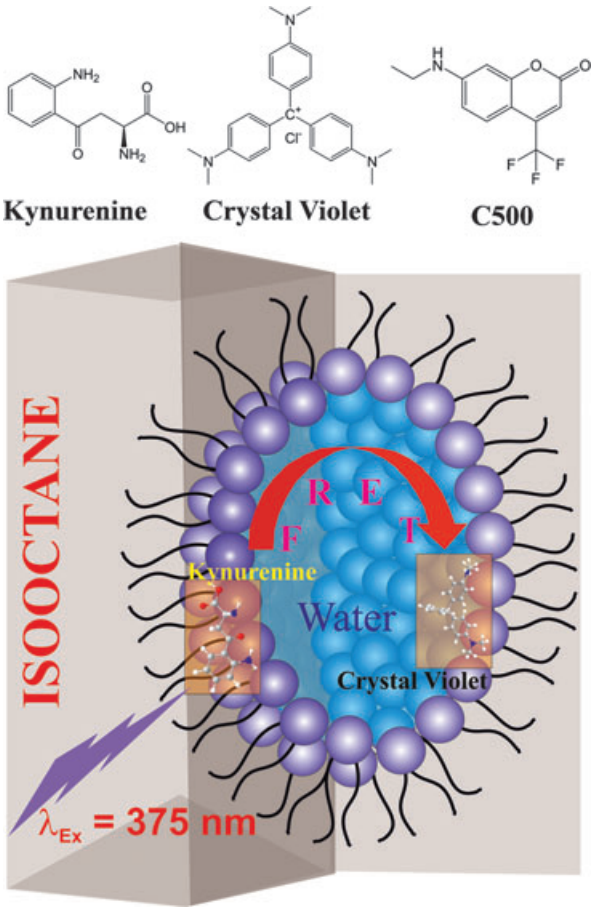

Scheme 1. The chemical structures of the probe molecules used in our studies are shown in the upper panel. The schematic representation of the FRET in Brij 30 RM is depicted in the lower panel. FRET = Förster resonance energy transfer.

the probe molecules with the degree of hydration of the RM. It has to be noted that we have done a similar study by using another well-known fluorophore, C500 and the result is similar with the KN-CV FRET experiment (tabulated in Table 4). The relative location of the donor (KN) with respect to the acceptor (CV) in the Brij 30 RM is shown in Scheme 1.

CONCLUSION

In summary, we have reported the relaxation dynamics of KN in a nonionic Brij 30 RM system and compared the results with a well-known solvation probe H33258 in the restricted environments. While DLS studies confirm the structural integrity of the RM, picosecond-resolved fluorescence anisotropy and the FRET of the probe KN confirm the location of KN in the interface of the RM. Our detail spectroscopic studies clearly indicate that the intermolecular (solute–solvent) hydrogen bonding dynamics of the probe KN leading to the IC of the probe in the restricted environments is much faster compared to the relaxation of the solvent molecules around it (solvation). These results suggest that the interfering excited state hydrogen bonding dynamics of the probe hinders the interrogation of slower environmental relaxation in the Brij 30 RM using KN.

Acknowledgements—S.R. and N.G. thank CSIR, India, for the fellowships. We thank DST, India, for a financial Grant (SR/SO/BB-15/2007).

SUPPORTING INFORMATION

Additional Supporting Information may be found in the online version of this article:

Figure S1. Fluorescence spectra of KN in Brij 30 RM at w_0 = 0 (black) and the empty RM (gray).

Figure S2. Excitation spectra of KN in Brij 30 RM at $w_0 = 0$ over the whole emission spectrum of KN. Gray dash line represents the normalized absorbance spectrum of KN in Brij 30 RM at $w_0 = 0$.

Figure S3. Solvent correlation function, $C(t)$ of KN in Brij 30 RM at different w_0 values indicates the faster dynamics with increasing water pool size.

Figure S4. Fluorescence decay transients of KN in Brij 30 RM at $w_0 = 0$ with 409 nm excitation.

Please note: Wiley-Blackwell is not responsible for the content or functionality of any supporting information supplied by the authors. Any queries (other than missing material) should be directed to the corresponding author for the article.

REFERENCES

1. Goswami, N., A. Makhal and S. K. Pal (2010) Toward an alternative intrinsic probe for spectroscopic characterization of a protein. *J. Phys. Chem. B* **114**, 15236–15243.
2. Pal, S. K. and A. H. Zewail (2004) Dynamics of water in biological recognition. *Chem. Rev.* **104**, 2099–2123.
3. Shen, X. H. and J. R. Knutson (2001) Subpicosecond fluorescence spectra of tryptophan in water. *J. Phys. Chem. B* **105**, 6260–6265.
4. Heyningen, R. V. (1971) Fluorescent glucoside in the human lens. *Nature* **230**, 393–394.
5. Sherin, P. S., J. Grilj, Y. P. Tsentalovich and E. Vauthey (2009) Ultrafast excited-state dynamics of kynurenine, a UV filter of the human eye. *J. Phys. Chem. B* **113**, 4953–4962.
6. Sherin, P. S., J. Grilj, L. V. Kopylova, V. V. Yanshole, Y. P. Tsentalovich and E. Vauthey (2010) Photophysics and photochemistry of the UV filter kynurenine covalently attached to amino acids and to a model protein. *J. Phys. Chem. B* **114**, 11909–11919.
7. Brubach, J. B., A. Mermet, A. Filabozzi, A. Gerschel, D. Lairez, M. P. Krafft and P. Roy (2001) Dependence of water dynamics upon confinement size. *J. Phys. Chem. B* **105**, 430–435.
8. Banerjee, D. and S. K. Pal (2006) Ultrafast charge transfer and solvation of DNA minor groove binder: Hoechst 33258 in restricted environments. *Chem. Phys. Lett.* **432**, 257–262.
9. Downs, T. R. and W. W. Wilfinger (1983) Fluorometric quantification of DNA in cells and tissue. *Anal. Biochem.* **131**, 538–547.
10. Pal, S. K., L. Zhao and A. H. Zewail (2003) Water at DNA surfaces: Ultrafast dynamics in minor groove recognition. *Proc. Natl Acad. Sci. USA* **100**, 8113–8118.
11. Moilanen, D. E., E. E. Fenn, D. Wong and M. D. Fayer (2009) Water dynamics in large and small reverse micelles: From two ensembles to collective behavior. *J. Chem. Phys.* **131**, 014704–014709.
12. Horng, M. L., J. A. Gardecki, A. Papazyan and M. Maroncelli (1995) Subpicosecond measurements of polar solvation dynamics: Coumarin 153 revisited. *J. Phys. Chem.* **99**, 17311–17337.
13. Lakowicz, J. R. (1999). ed., *Principles of Fluorescence Spectroscopy*. Kluwer Academic/Plenum Publishers, New York.
14. Sarkar, R. and S. K. Pal (2006) Ligand-DNA interaction in a nanocage of reverse micelle. *Biopolymers* **83**, 675–686.
15. Koti, A. S. R., M. M. G. Krishna and N. Periasamy (2001) Time-resolved area-normalized emission spectroscopy (TRANES): A novel method for confirming emission from two excited states. *J. Phys. Chem. A* **105**, 1767–1771.
16. O'Connor, D. V. and D. Philips (1984) *Time Resolved Single Photon Counting*. Academic Press, London.
17. Wu, P. and L. Brand (1994) Resonance energy transfer: Methods and applications. *Anal. Biochem.* **218**, 1–13.
18. Mitra, R. K., S. S. Sinha, P. K. Verma and S. K. Pal (2008) Modulation of dynamics and reactivity of water in reverse micelles of mixed surfactants. *J. Phys. Chem. B* **112**, 12946–12953.
19. Churchich, J. E. (1972) L-kynurenine: A fluorescent probe of serum albumins. *Biochim. Biophys. Acta* **285**, 91–98.
20. Fee, R. S. and M. Maroncelli (1994) Estimating the time-zero spectrum in time-resolved emission measurements of solvation dynamics. *Chem. Phys.* **183**, 235–247.
21. Kalninsha, K. K., D. V. Pestova and Y. K. Roshchina (1994) Absorption and fluorescence spectra of the probe Hoechst 33258. *J. Photochem. Photobiol. A* **83**, 39–47.
22. Santhanalakshmi, J. and S. Balaji (2001) Binding studies of crystal violet on proteins. *Colloids Surf. A* **186**, 173–177.